

# UTILIZATION OF MARS GLOBAL SURVEYOR ACCELEROMETER DATA FOR ATMOSPHERIC MODELING

R. H. Tolson<sup>1</sup>, G. M. Keating<sup>2</sup>, S. N. Noll<sup>3</sup>, D. T. Baird<sup>3</sup>, T. J. Shellenberg<sup>3</sup>

## Abstract

To provide safe aerobraking for the Mars Global Surveyor mission, accelerometer data were utilized for near real time determination of atmospheric density and scale height. These measurements, when properly calibrated, will provide the initial data base for improvement of Mars thermospheric models. Calibration methods including adjustments for thruster firings and multi-body dynamics are presented. Some unanticipated results are shown of possible atmospheric “shocks” and standing planetary waves.

## Introduction

The Mars Global Surveyor (MGS) was the first planetary spacecraft to rely on aerobraking as an enabling technology for mission success.<sup>1</sup> During the MGS Aerobraking Peer Review in Feb. 1995, the orbit to orbit variability in density at aerobraking altitudes at Mars was estimated at 70%  $2\sigma$ . In addition, a global Martian dust storm could produce factor of 2 or more increases in density.<sup>2</sup> As a result of these estimates, MGS drag was increased by adding “drag flaps” to the end of each solar array as shown in Figure 1. The increased drag permitted the maintenance of the planned orbital period profile while decreasing aerodynamic heating of the temperature sensitive solar arrays. During the early phases of MGS aerobraking it was found that natural variability was actually very close to the pre-flight estimate, and that predictions based on past orbits using either relatively simple empirical models<sup>3</sup> or a sophisticated model,<sup>4</sup> had a remaining variability of about 60%  $2\sigma$ . Further, a regional dust storm occurred in Nov. 1997 on orbit 51 producing a 133% increase<sup>1</sup> in density from the previous orbit. MGS encountered unpredicted planetary longitudinal waves<sup>1,3</sup> with maximum to minimum density ratios greater than three within 75 degrees of longitude. These standing waves appear to be correlated with Mars topography<sup>5</sup> and season. Finally, changes in atmospheric density by large factors were found to occur over spatial scales of a few kilometers. After this early MGS aerobraking experience, the Mars Climate Orbiter allocated 80%  $2\sigma$  for orbit to orbit variability independent of dust storms.

Such large uncertainties in the atmospheric environment result in payload penalties and/or increased operations cost for all future Mars aerobraking missions. Therefore, developing and improving atmospheric models for the Mars thermosphere is highly desirable. Accelerometer data from the MGS aerobraking phases provide the beginnings of a data base that can be used to generate models of the Martian thermosphere from approximately 110 km to 170 km. The MGS data set provides limited seasonal/latitudinal coverage and should therefore be complemented with accelerometer and orbit decay data

---

Professor, School of Engineering and Applied Sciences, George Washington University, JIAFS, NASA LaRC, Hampton, VA 23681.

<sup>2</sup>Senior Research Staff Scientist, School of Engineering and Applied Sciences, George Washington University, JIAFS.

<sup>3</sup>Graduate Research Scholar Assistant, George Washington University, JIAFS.

from other Mars missions. Density derived from orbital decay is limited to a single measurement per orbit and the accuracy is limited by the lack of knowledge of atmospheric scale height or temperature. Accelerometer data provide direct measurements of scale heights and densities over a range of altitudes on each pass. Unfortunately, individual missions do not necessarily appreciate the importance of accelerometer data to subsequent Mars missions, and consequently the quality and quantity of data returned may be only the minimum to assure success for that particular mission.

The utilization of accelerometer data by the George Washington University Accel Team for MGS operations<sup>3</sup> only required density recovery from periapsis to about two scale heights (10 to 20 km) above periapsis. For the development of models, it is desirable to refine the operational procedures to improve and extend density recovery to the highest possible altitude. Before this improvement can take place, there are various issues affecting the data that must be overcome to assure accurate results. These issues include thruster activity, multi-body dynamics due to the cracked solar array, high frequency signals of varying frequency due to solar panel vibration,<sup>3</sup> and nearly instantaneous changes in dynamic pressure due to unknown sources. This paper will discuss the methods used to ameliorate

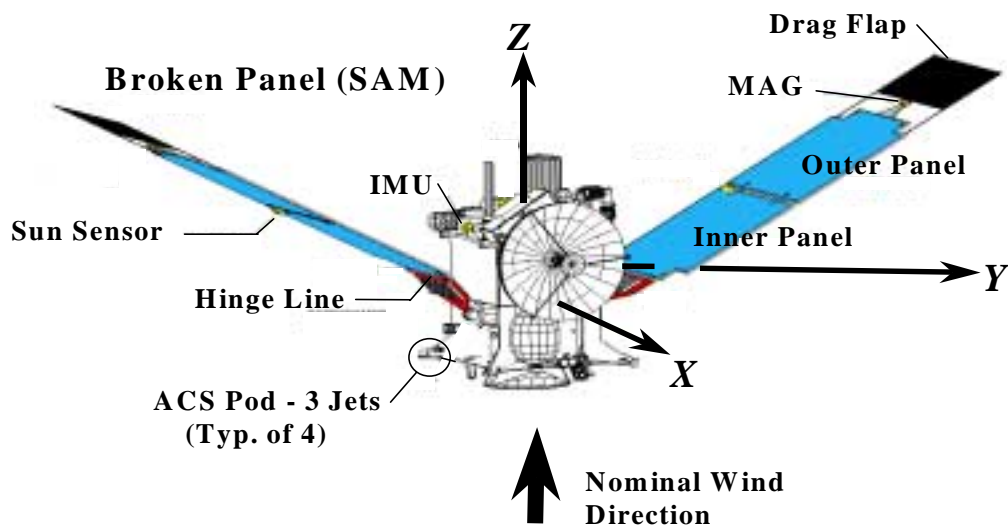


**Figure 1 Mars Global Surveyor in aerobraking configuration.**

these effects and to process the MGS accelerometer data for submission to the NASA data archives.

### Spacecraft and Data

MGS is shown in the aerobraking configuration in Figure 1. The solar array on the minus y-axis (SAM) has a cracked yoke. The discovery of this crack<sup>1</sup> led to the division of aerobraking operations into Phase 1 (9/97-3/98) and Phase 2 (9/98-2/99). Four sets of 3 thruster jets maintained attitude control during each aerobraking pass. Three (2 parallel to z and 1 for roll about z) are on the ends of the four arms at the -z end of the spacecraft.

### *MGS Accelerometer Data*

Four accelerometers (x,y,z and skew) along with 4 gyros are contained in the IMU located on the nadir deck shown in Figure 1. The only accelerometer used in the aerobraking analysis was the z-axis accelerometer. The accelerometers are Sundstrand QA1200-AA08 Q-Flex which continuously integrate acceleration to obtain velocity change. The instrument is sampled at 10 Nyquist (  $N_q$ =samples/second) and the data are recorded in instrument counts or quantized velocity increments equivalent to 0.332 mm/s per count. The accelerometer bias has a specified temperature sensitivity of 10  $\mu$ g/K or approximately 0.3 counts/K. Temperature within the IMU is actively controlled. Nevertheless, there are orbits that show drifts in bias and shifts between inbound and outbound portions of the orbit while the s/c is not subject to significant aerodynamic forces. The largest differences between inbound and outbound bias was about 0.2 counts and drifts never exceeded  $10^{-3}$  counts/second. Such small differences could be safely ignored during operations but have been considered for data archiving.

The z-accelerometer sampling rate during the aerobraking phase was originally set at 10 contiguous 0.1-second measurements every 8 seconds. This sample rate was based on simulations<sup>6</sup> that indicated density could be recovered with at least 3% accuracy at nominal aerobraking altitudes assuming no aerodynamic coefficient errors. Aerodynamic coefficients were generated using a direct simulation Monte Carlo technique for transitional flow<sup>7</sup> After the hiatus (P19-P37) to evaluate the implications of the excessive SAM deflection on orbit 15,<sup>1</sup> the data rate was increased on orbit 40 to 10  $N_q$  to improve atmospheric recovery and also to monitor the dynamics of the SAM. There were a number of orbits from P911 to P961 where the telemetry was cut in half due to one of the on board computers going off line. Only data at the higher sample rate are being archived. There are also a few orbits from which no telemetry was received.

The fundamental equation used to derive atmospheric density is

$$a_{\perp} = \frac{\rho V^{\perp} C_{\perp} A}{2m} \quad (1)$$

Upon arrival at Mars, MGS had a mass of  $m=763$  kg and ended the aerobraking phase with a mass of 751 kg. An average value of 757 kg has been used for density recovery. Extensive discussions of the calculation<sup>7</sup> of the axial force coefficient  $C_z$  and the utilization<sup>6</sup> of  $C_z$ , including the iterative process to account for SAM quasi-static deflection during aerobraking are given elsewhere. Since  $C_z \approx 2$ ,  $A=17.04$  m<sup>2</sup>, and periapsis velocities during aerobraking decreased from 4.8 to 3.6 km/s, one accelerometer count/sec (0.332 mm/s<sup>2</sup>) is approximately

equivalent to a density of 0.6 and 1.1 kg/km<sup>3</sup>, respectively. The accelerometer accumulates velocity changes so that density resolution can be increased at the expense of temporal and spatial resolution.

### *Auxiliary Measurements*

Body angular rates and attitude quaternions were recorded at 1 Nq. Rates were digitized at a resolution of 1  $\mu$ rad/sec. Attitude rate data is passed through an onboard low pass filter with a 2 Hz cut off to alleviate structural mode coupling into the attitude control system. This filter introduces a frequency dependent delay. This delay is negligible for the low frequency body motion provided by aerodynamic stability, but introduces a 1.2 second delay for the 0.16 Hz vibration signal due to SAM vibration and 2 seconds for impulses like thruster firings.

While aerobraking, attitude control corridors were expanded and thrusters were utilized to maintain the attitude within these widened corridors. The spacecraft is neutrally stable to rotation about the z-axis, so that the most frequent firings were the jets about z. These four jets are coupled and orthogonal to the z-axis and no direct input into the z-accelerometer was ever detected. Due to the swept solar arrays, the spacecraft is longitudinally stable about both x and y axes. With only a couple of exceptions, thruster firings to control rotation about these axes occurred as the spacecraft was on the outbound portion of the aerobraking pass. To control motion about x and y, the remaining eight thrusters fire parallel to the z-axis and the resulting accelerations often exceeded the atmospheric contribution to z-acceleration. Telemetry on thruster firings consisted of cumulative total firing times for each of the 12 thrusters sampled every 8 seconds. During operations the accelerometer measurements corresponding to the thruster data interval were replaced by a linear interpolation across the interval. A more refined definition of the location of thruster firings has been developed for archiving and will be discussed later.

### *Time Tagging the Data*

During the early part of operations it was found that the time tags on the three fundamental data types, accelerometer counts, attitude rates, and thruster firing times, were not synchronized. Information on the telemetry maps for all these data were not available. Five of the 10 accelerometer channels came from each of the two onboard computers and special care was taken to assure that these data were properly ordered in time. Accelerometer data time tags were taken as the fundamental reference and all orbital velocities and positions are interpolated to this time. Between Phase 1 and Phase 2 of aerobraking, it was found that the accelerometer time tags were delayed 1.5 seconds on the s/c and subsequently all accelerometer data were shifted 1.5 seconds relative to UTC. As mentioned above, attitude rates have a frequency dependent delay in addition to any basic uncertainty in time tagging. Finally, there is uncertainty in the proper time tags for thruster firing. To synchronize the rates and thruster data with the accelerometer data, numerous firings of the x- and y-thrusters throughout the mission were studied. Such thruster firings should produce simultaneous effects in rates and acceleration. By these means it was found that for the purposes herein,

the rate time tags required shifting by -2 seconds to be in synch with the already shifted accelerometer data. By studying thruster firings that occurred on either side of the 8 sec thruster data interval, it was concluded that the thruster time tag needed to be shifted by -0.5 seconds.

### *SAM Vibration*

One source of non-atmospheric z-acceleration was due to the vibration of the SAM. The fractured SAM oscillated about the assumed crack in the yoke.<sup>1</sup> The oscillation was essentially a rotation about an axis parallel to the x axis with a period between 5 and 7 seconds (Appendix). Only for the largest SAM oscillations was there even a hint of rotation about the y or z directions and this may have been due to inertia coupling or onboard momentum sources. At the crack, the connection between the SAM and the rest of the spacecraft (hereafter called the bus) acted like a non-linear torsional spring.<sup>6</sup> Consequently, SAM vibration reacted against the bus and induced motions of the bus that were detected by the accelerometer. During Phase 2 of operations these oscillations were removed by simply performing a 67 point running mean of the 10 Nq accelerometer data. The method for eliminating the SAM vibration from the accelerometer data for the archive data set will be discussed later.

*Sample Data Sets*

Figure 2 provides examples of the diversity of aerobraking profiles. The upper figures show raw 1 Nq accelerometer data for orbits 58 (P58) and 585 (P585). Through the entire mission the bias remained near 56.6 counts per second, where one count is 0.332 mm/sec. The lower plots show the attitude angular acceleration about the x-axis as inferred from a two sided derivative of the rate data. Each “\*” on the upper portion of the angular acceleration plot indicates times of x- and/or y-thruster activity. For P58, the first thruster firing shows as a large peak on both the counts and angular acceleration plots at about 130 seconds. A

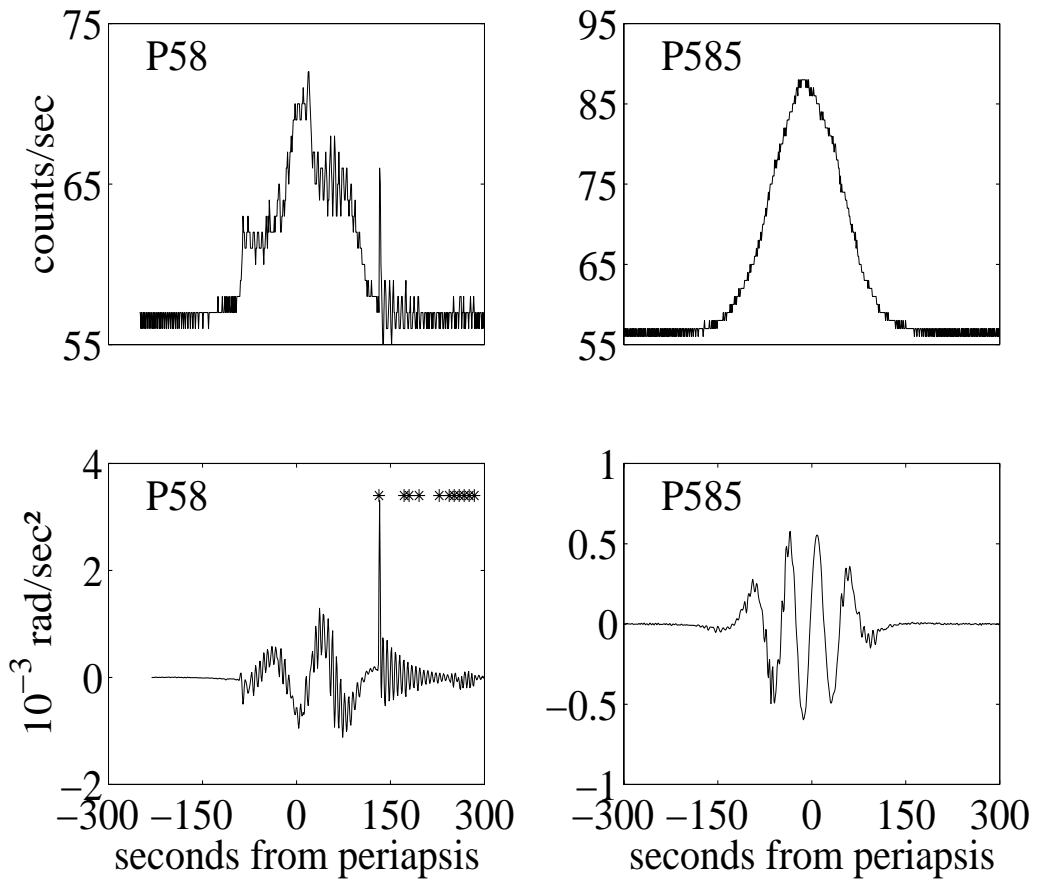


**Figure 2 Accelerometer counts and body angular acceleration about x-axis for orbits 58 and 585.**

residual damped oscillation of the SAM dominates the angular acceleration after the initial large thruster firing and the vibration appears in the acceleration data as well. Many of the subsequent thruster firings also appear in both data sets. Notice the factor of about five increase in counts above the bias that occurs near -90 seconds which also excites SAM

vibration. This region will be discussed in some detail later.

Orbit 585, on the other hand, has no x- or y-thruster activity while MGS is in the atmosphere, shows only a small amount of SAM oscillation, and does not have any sudden changes in acceleration. Textbook orbits like P585 were relatively rare during the course of MGS aerobraking.

### Data Reduction Procedures

Consider a coordinate system fixed in the bus with origin at the center of mass of the spacecraft when the SAM is in the nominal position. The measured acceleration is composed of a number of terms given by

$$\mathbf{a}_{\text{measured}} = \mathbf{a}_{\text{instrument}} + \mathbf{a}_{\text{aerodynamic}} + \mathbf{a}_{\text{gravity}} + \mathbf{a}_{\text{attitude}} + \mathbf{a}_{\text{angular}} + \boldsymbol{\omega} \times (\boldsymbol{\omega} \times \mathbf{r}) + \dot{\boldsymbol{\omega}} \times \mathbf{r} + \mathbf{a}_{\text{vibration}} \quad (2)$$

where the terms are respectively the measured accelerations due to the instrument bias, aerodynamic forces, gravity gradient, attitude control system thruster activity, angular motion of the accelerometer about the origin (2 terms), and translational motion of the accelerometer due to SAM vibration. Gravity gradient is negligible and will not be discussed further.

### *Thruster Firings*

Commands to fire thrusters are generated every cycle (0.5 seconds) by the onboard computer. Firing time is a multiple of 1/32 seconds with a maximum firing time of 0.25 seconds per cycle. It was not uncommon to have firings in contiguous computer cycles, but seldom, if ever, did three consecutive cycles have firings. For short burns, impulse is not linear in firing time due to blow down and initial catalyst temperature. Nevertheless, an attempt was made to calibrate the thrusters using the change in angular rates. For burn times between 0.2 and 0.5 seconds, rms deviation in equivalent thrust was about 12%. Deviation rapidly increased as burn time decreased becoming 70% for firing times less than 0.07 seconds. The large deviation appeared to be related to the time since the previous burn, suggesting that the temperature of the catalyst bed at the initiation of the burn is a major factor in determining efficiency for such short burn times.

Without a reliable calibration method, it was decided to continue with the practice of replacing thrust corrupted acceleration data. However both the method for locating the corrupted data and the method for replacing the data were improved. The time of thruster firing within the 8 second interval was found by studying the attitude rate data. If the thruster or thrusters produced any component of torque about the y-axis, the time of firing could generally be identified within  $\pm 1$  sec by finding the location of maximum angular acceleration within the 8 sec interval. In this case a group of only three accelerometer data points were identified for replacement. Multiple non-contiguous firings, though rare, were also easily identified in this case. If a pair of thruster firings only produced a torque about the x-axis, the same method did not produce as reliable an estimate because the SAM

vibration excited by the thruster firing corrupted the angular rate measurement after the firing. This case typically led to groups of 4 to 6 points being identified for replacement. If small x-only firings occurred while the SAM was already vibrating, the resolution of the time of thruster firing was occasionally reduced to such a point that all 8 points were identified for replacement.

During operations all 8 accelerometer points within the thruster telemetry frame were replaced with interpolated values from a linear model fit to adjacent accelerometer data. For archiving the following method was used. Since the x-y thruster firings always occurred after the s/c has begun aerobraking, the data were replaced starting with the latest group designated for replacement and moving group by group toward periapsis to the earliest group. First, an outbound bias was determined from the average of the outbound accelerometer data “outside” the atmosphere and not marked for replacement. All data “outside” the atmosphere are then replaced by simulated quantized data with a mean value equal to the outbound bias. Simulated quantized data are utilized in lieu of a constant because the next step in the process will require filtering of the data and changes in data structure will produce artifacts. Remaining groups of data to be replaced can have an atmospheric contribution, so these groups are replaced by data from a model fit to 15 data points on either side of the group to be replaced. The model assumes counts are exponentially related to altitude with a constant scale height. The upper part of Figure 3 shows the accelerometer data after the thruster corrupted data are replaced. Note that the large acceleration near 130 seconds has been replaced, but the contribution due to SAM vibration remains.

### *SAM Vibration*

The last term in Eq. 2 is the only term for which there are no direct measurements. The vibrations of the SAM react against the bus to produce angular and translational motion of the bus. The angular contribution is included in the two previous terms. If there were no external torques or forces, conservation of linear and angular momentum can be used to show<sup>6</sup> that this translational contribution is proportional to the  $\dot{\omega}_v$  of the bus induced by the vibration. This component of the total angular acceleration can be obtained by differentiating and high pass filtering the measured body rates to obtain only the contribution due to the vibration. This approach requires knowledge of the location of the crack in the yoke and ignores other effects that contribute to the dynamic interaction of the bus and SAM. Using best estimates of crack location, the method accounts for 90% of the total contribution of the SAM vibration to the measured z-acceleration. This deficiency could be due to the onboard filtering of the attitude rates as well as neglected dynamics such as fuel sloshing and aerodynamics.

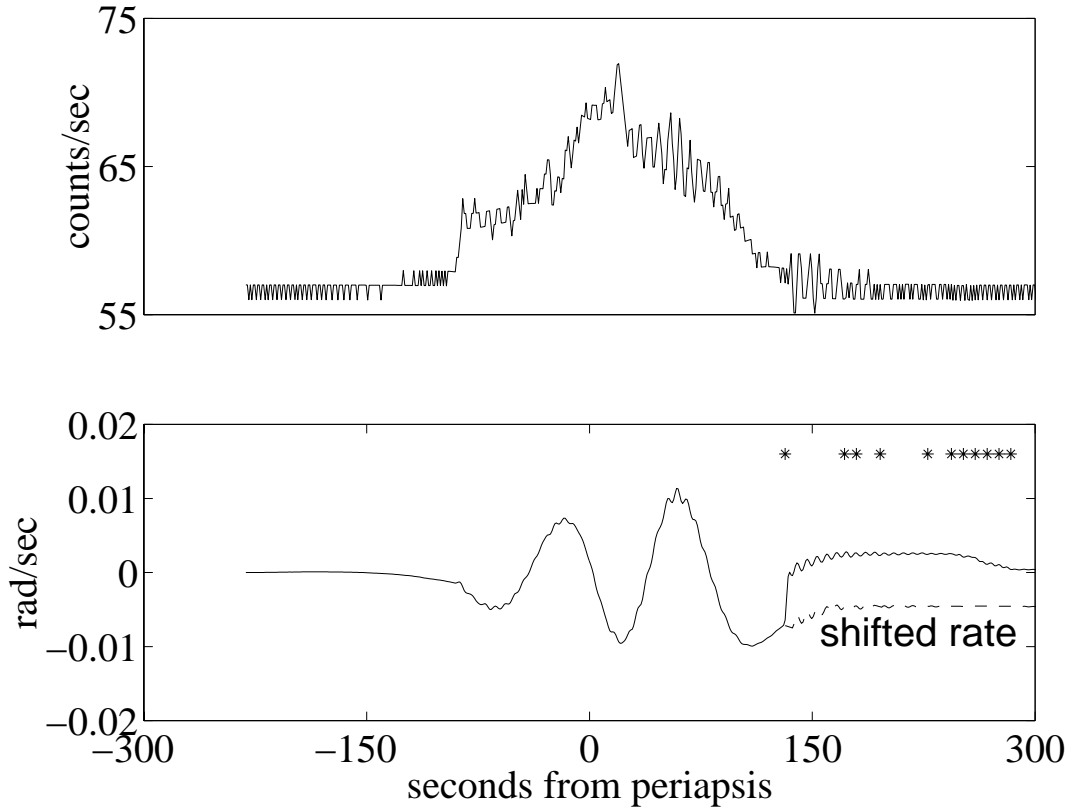


**Figure 3 Accelerometer counts with thruster corrupted data replaced for P58. Shifted and unshifted  $\omega_x$ , for P58.**

Such a linear relation between the vibration induced angular acceleration and resulting z-acceleration is the basis of an alternate approach which does not require knowledge of s/c physical properties or more sophisticated dynamics. In this approach it is noted that the last two terms in Eq. 2 are linear in angular acceleration induced by the vibration. Further, as seen in Figure 2, the angular motion of the spacecraft is composed of contributions due to aerodynamic torques with characteristic periods of oscillation greater than 30 seconds (0.03 Hz) and contributions due to SAM vibration with a period near 6 seconds (0.16 Hz). This large frequency difference permits straight forward separation of the two contributions. The x-angular rate is filtered to produce a high frequency component that captures the SAM vibration and a low frequency component that captures the contribution due to aerodynamic moments. Likewise the accelerometer data, with thruster corrupted data points replaced, is high pass filtered. All filtering is done forward and backward to eliminate phase shifting using a finite impulse response filter with 40 taps and a frequency cut off at 0.075 Hz. To reduce Gibbs phenomena in the high pass results at thruster firings, the  $\omega_x$  is first “shifted” at the already identified times of thruster firing to provide linear continuity across the time allocated for the firing. A sample of the original rates and the shifted rates are shown in the lower part of Figure 3. The shifted rates are only used for input to the high pass filter. The final step is to relate the high pass acceleration to the high pass x-angular rate and x-angular

acceleration through the linear regression

$$\tilde{a}_{\perp} = \alpha \tilde{\omega}_{\perp} + \beta \dot{\tilde{\omega}}_{\perp} \quad (3)$$

where the tilde denotes high pass filtered data. The angular rate term is included as a quadrature signal to absorb any remaining time difference between the acceleration and rate data. This contribution is then subtracted from the accelerometer counts. Plots of the regression coefficients for each orbit are shown in Figure 4. The mean value of  $\alpha$  is -221, with a rms deviation of 204 and the mean value of  $\beta$  is -3670 with a rms deviation of 240. There appears to be a shift in  $\beta$  after orbit 1000 which is not understood as yet. The large scatter from orbits 560 to 1000 is due to most thruster firings occurring late on the outbound leg and to the limited amount of SAM oscillation that occurred during the aerobraking pass.

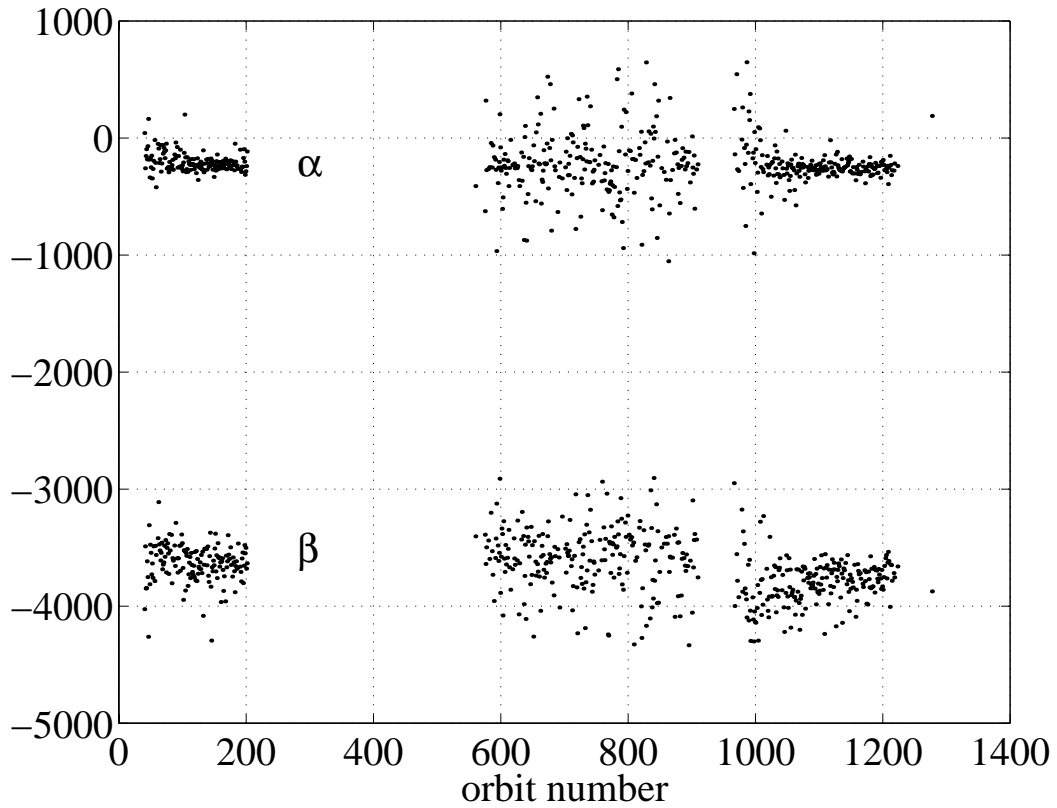


**Figure 4 Coefficients of linear regression of high pass acceleration and body angular motion.**

For orbit 58, the resulting counts are shown as the upper, curve in Figure 5 identified as “No averaging”. The bias has been removed and the curve shifted 5 counts for clarity. The correction has significantly reduced the SAM vibration contribution after the  $t=-90$  sec transient and after the major thruster firing at  $t=130$  sec. For times earlier than  $t=-90$  and

later than  $t=250$ , the data are essentially the raw counts. Between these time the various corrections have replaced the quantized data with a signal with about the same noise level. It might be suggested that this process is equivalent to just subtracting the high pass accelerometer signal from the original signal. Such a process would smooth or remove all transient atmospheric phenomena like that near  $t=-40$  seconds, which is probably a density wave. The process above only removes transients that correlate with SAM vibration.

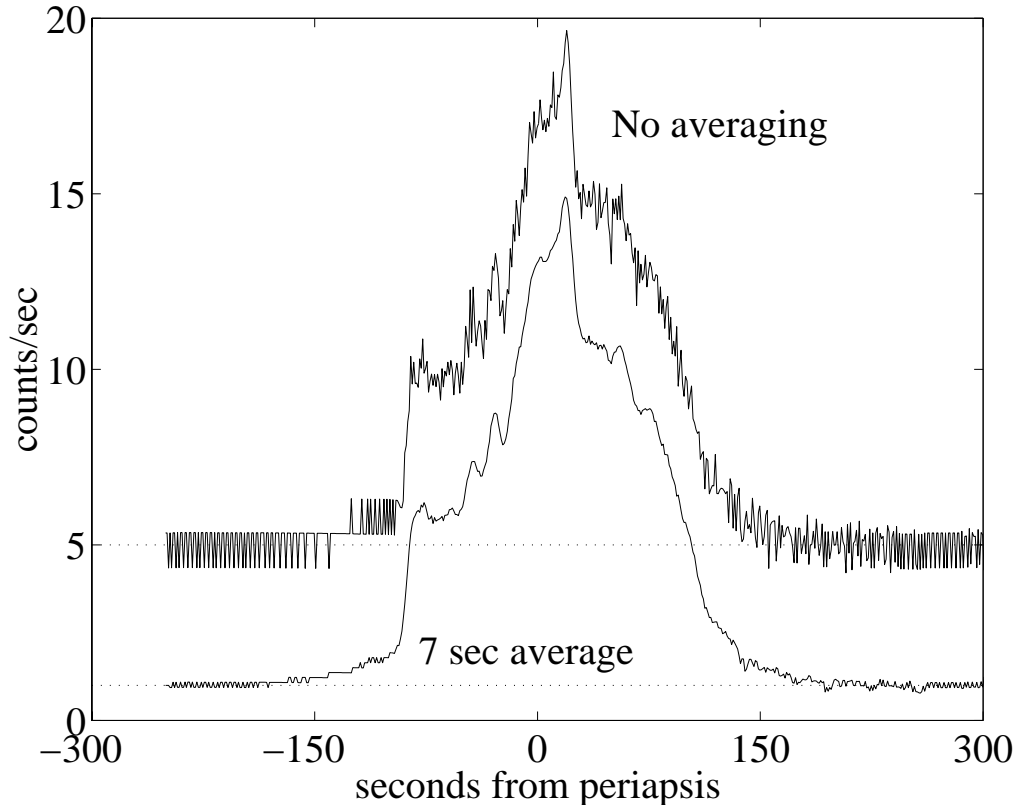


**Figure 5 Accelerometer data after SAM vibration removed and after 7 point running mean.**

The original plan was to archive densities derived from these data; however, such densities would have a considerable noise component due to quantization and numerous “negative” densities once the bias is removed. Instead it was decided to archive two averaged densities. The first is derived by averaging the “No averaging” accelerometer counts over 7 seconds. This averaging interval is close to the period of oscillation of the SAM and should reduce any remaining signal from the SAM vibration. The result of this averaging is shown in the lower part of Figure 5. There will still be negative counts and these will be converted into negative densities for the second averaging process to be discussed later. Densities derived from the 7 second average are not archived before the last negative count inbound and after the first negative count outbound.

*Quality Indicator*

Both the replacement of data to account for thruster firings and the corrections for SAM vibration are based on an empirical approach rather than strict mathematical, physical or statistical principles. Nevertheless, these data should not carry the same weight in determining atmospheric models as data that required no corrections. Consequently, an empirical quality indicator (QI) was developed to identify potential lower quality data because of the corrections. QI was initially set to unity for each data point and can be thought of as a normalized variance. Data replaced due to thruster firing are given a QI=3. The QI is also inflated for data adjusted for SAM oscillation using the linear regression in Eq. 3 by  $QI=1+0.4|\tilde{a}_z|$ . This acknowledges about 20% error in the correction, for example, accelerometer corrections of 2 counts similar to P58 near t=50 in Figure 3 would lead to QI=1.8. The third adjustment to the QI accounts for the rare situations where the MGS attitude relative to the wind was outside the range of values in the aerodynamic tables. The tables<sup>7</sup> covered deviation from the relative wind of up to 15°. On a few orbits this limit was exceeded by up to 5 degrees. These violations usually occurred either early on the inbound leg or late on the outbound leg where aerodynamic stabilizing torques were negligible. In any case, the value of  $C_z$  used for density recovery is the value at the boundary of the table. At the boundary of the tables, changes in  $C_z$  are less than 0.007 per degree, depending on density, heading and SAM deflection.<sup>6</sup> The QI for points outside the table are inflated by 0.014 per degree beyond the boundary.

The final contributor to QI attempts to account for navigation errors. Doppler tracking of MGS was not possible in the aerobraking orientation. The most accurate orbit determination occurred when tracking data on both sides of the aerobraking pass were included in the solution. In this case the orbit was called “reconstructed.” Orbits that were not reconstructed were tagged R+1, R+2, etc depending on how many orbits lapsed since the last reconstruction. The main contribution of navigation errors to density recovery is in the calculation of altitude. Experience during the mission showed that periapsis altitude could be reconstructed and predicted within 100 meters for at least two orbits. Such an error introduces less than 5% error in equivalent density since density scale height is generally greater than 5 km. Accuracy of predicting the time of periapsis rapidly degraded with the number of orbits predicted because of the uncertainty in the density on subsequent passes. For example, from P41 to P194 the orbital period was reduced by 23.2 hrs,<sup>1</sup> for an average period reduction of 544 sec/orbit. A 20% deviation in density from the assumed value for the R+1 orbit would result in over 100 seconds error in the time of periapsis on the R+2 orbit. On the other hand, prediction on the R+1 orbit were generally within a second because the effects of atmospheric errors during the inbound leg had less than 200 seconds to accumulate. The time of maximum density or dynamic pressure could not be used to precisely locate periapsis since this time often deviated by 10 seconds or more from reconstructed periapsis times due to latitudinal density gradients and geodetic altitude. Nevertheless, the dynamic pressure was the only available indicator of periapsis, so for R+n, n>1 type orbits, the time of periapsis was shifted to coincide with the time of maximum dynamic pressure, as measured by the accelerometer. For these orbits, the QI is set to reflect the error in altitude away from periapsis due to an error in the time of periapsis of 10 seconds. The error is proportional to the altitude rate times 10 seconds. This error in altitude is mapped into an equivalent fractional density error by assuming a seven kilometer

scale height and QI is inflated by the square of this result. For example, on orbit 755, the earliest R+2 type orbit, altitude rate at  $h=200$  km was 0.53 km/s leading to a  $QI=3.5$ . Of course, lower altitudes have lower values of QI becoming unity at periapsis. The time of periapsis correction has less influence on the QI as the orbit becomes less eccentric later in the mission. Even though these data are down weighted, it should be noted that an actual error in time of periapsis will produce a bias between inbound and outbound altitudes that might be misinterpreted as a latitudinal gradient.

The final QI is obtained for each data point by multiplying the four contributions above. QI for averaged data is obtained by applying the same averaging process to QI as to the data.

### Density Recovery

The 7 sec averaged counts are converted into density values using Eq. 1 by an iterative procedure<sup>3</sup> to simultaneously determine the quasi-static SAM deflection so that  $C_z$  can be obtained from the aerodynamic tables. Results for orbit 58 are shown in Figure 6 and tagged with  $\rho_7$ . For these data, a single bias is determined using both inbound and outbound 7 sec averaged counts above the atmosphere. There were generally more than 100 points used for this application. The random error in these 1 Nq samples is about one half the digitization level (approximately 0.3 kg/km<sup>3</sup> early in the mission to 0.5 kg/km<sup>3</sup> late in the mission) or

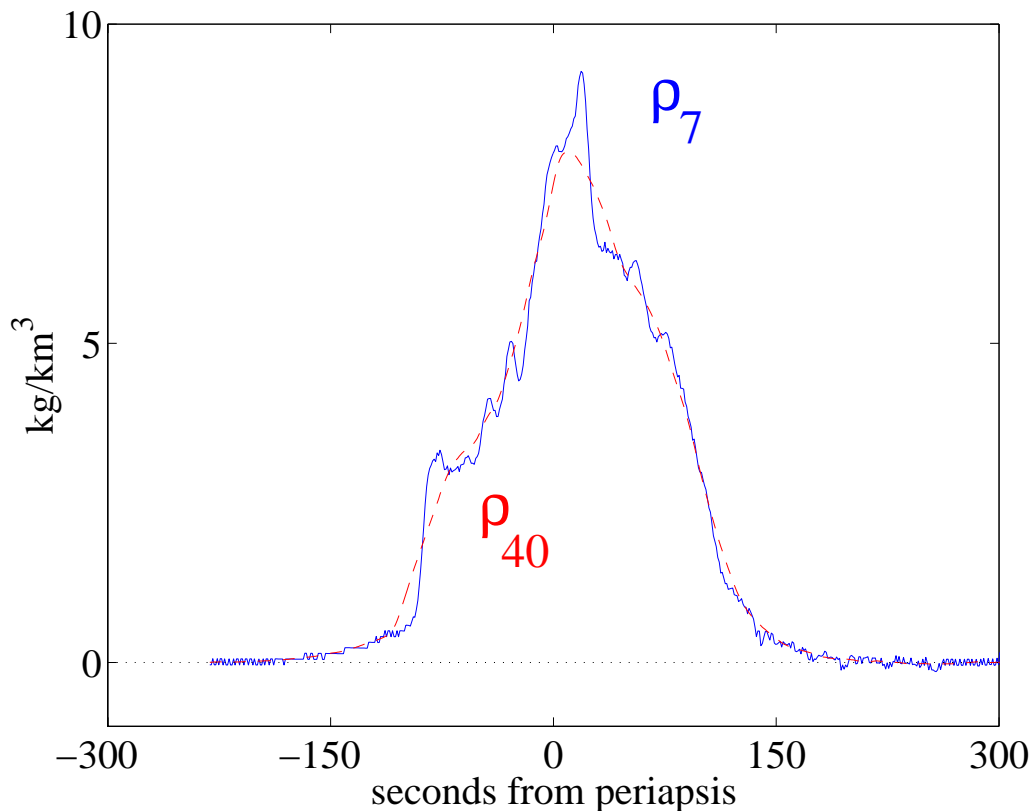
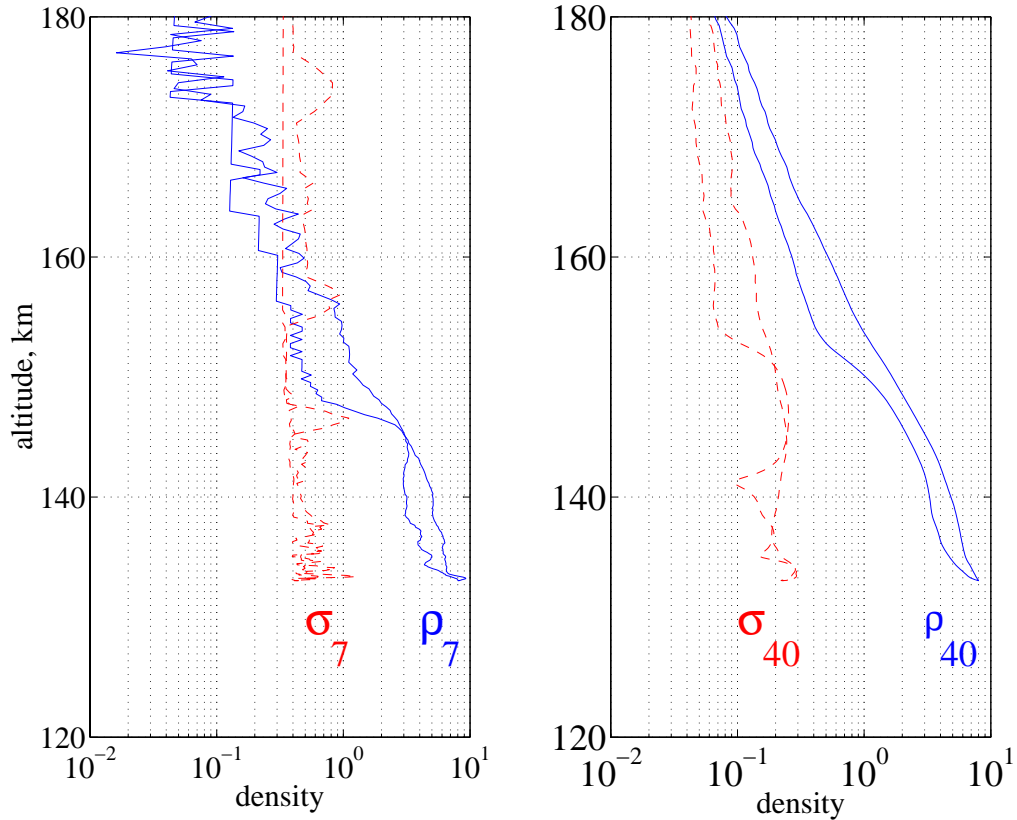


Figure 6 Comparison of 7 and 40 second density results.

every seventh point can be considered independent with an error between 0.06 and 0.1 kg/km<sup>3</sup>.

For many orbits, there is still considerable wave structure in these data which do not represent the “mean” thermosphere. So a second data set, tagged  $\rho_{40}$  in Figure 6, is also archived. This data set is the 40 point running mean of  $\rho_7$ .



**Figure 7 Density variation with altitude and errors.**

Figure 7 shows the variation of  $\rho_7$  and  $\rho_{40}$  with altitude along with error estimates. A formal error estimate is calculated for both  $\rho_7$  and  $\rho_{40}$  and denoted  $\sigma_7$  and  $\sigma_{40}$ , respectively. The former is the product of the estimated standard deviation of the mean based on the root mean square deviation of the 7 accelerometer points that were used to produce each of the smoothed counts in Figure 6 and the square root of the seven point mean of QI. The estimate

is mapped into density using Eq. 1. Note the regions near altitudes of 145 and 155 km where the QI has inflated the error due to replacement of data corrupted by thruster firings. The value of  $\sigma_{40}$  is determined likewise based on the deviation of the 40 point running mean of  $\rho_7$ . The two sets of densities are archived for all contiguous data points where the density is greater than one half of the corresponding sigma. The errors associated with each data point are dominated by quantization and natural variability and should be considered more of an indicator of relative accuracy rather than absolute accuracy. Areo-location data are also supplied with each data point including altitude above the (4,4) potential surface, areodetic latitude, longitude, local solar time, solar zenith angle and time from periapsis.

The final data products are densities and density scale heights provided at reference altitudes of periapsis, 130, 140 150, and 160 km. The later 4 are obtained by a least squares fit to the  $\rho_{40}$  data sets that span 5 km on either side of a reference altitude for both the inbound and outbound portions of the orbit. The values at periapsis are obtained by a similar fit to all data within 10 km of the periapsis altitude. Figure 8 shows examples of these results for P58 and P585. Note that for P58 there is no data at 130 km.

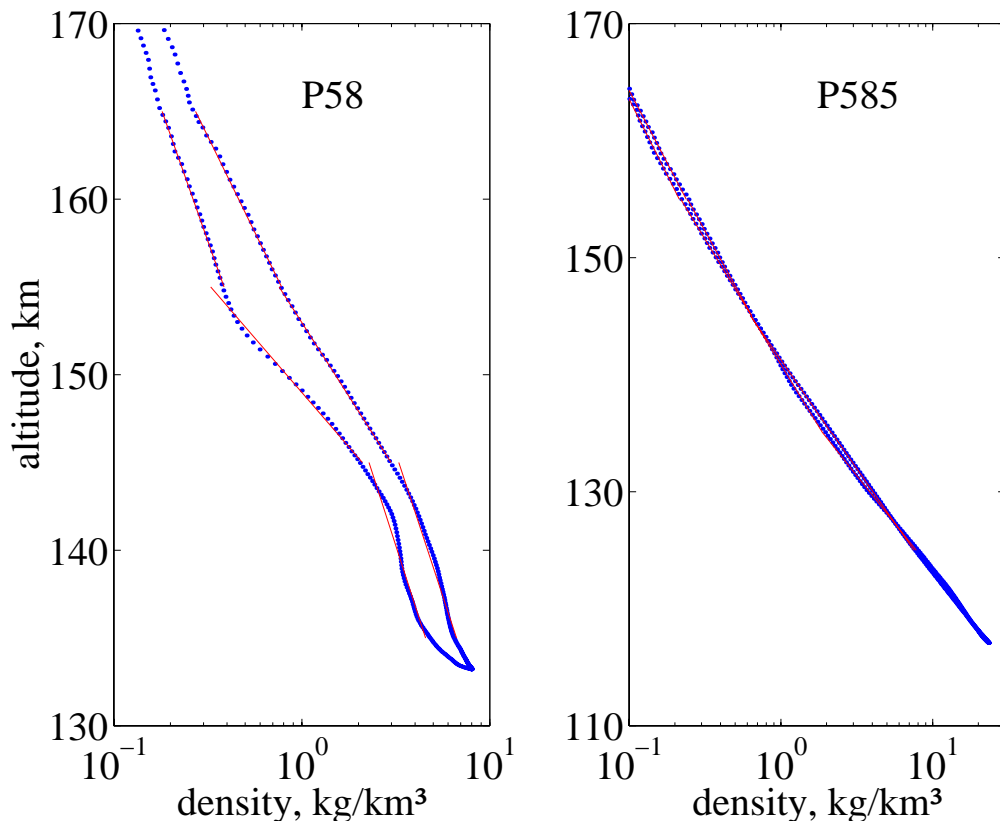


**Figure 8 Reference altitude density and scale height models for orbits 58 and 585.**

P585 shows little difference between inbound and outbound density profiles and the log linear fits to the profiles well represent the altitudinal variation over the 10 km altitude range of the fits. The outbound leg of orbit 58 gives densities between 50% and 100% larger than

the inbound leg. This is generally interpreted as a latitudinal gradient in density. Latitudinal gradients in temperature have also been found on a number of orbits.<sup>3</sup> The log linear fits for P58 provide reasonable representations to the local density and density scale heights; but, it is clear that if the reference altitude had been 145 or 155 km, the representation would have not been as faithful. Even with the 40 second averaging, care must be exercised when interpreting the reference altitude results for orbits with considerable wave activity.

## **Wave Phenomena**

Probably one of the most unexpected phenomena in the Mars thermosphere was the extensive wave activity. These variations occurred over dramatically different spatial and temporal scales. Standing planetary scale, longitudinal waves were found to persist over extended periods of time that may include an entire Mars season. At the other end of the spectrum, sudden changes in density of more than a factor of 2 occurred over spatial scales of less than 25 km horizontally and a kilometer vertically. Such rapid variations might eventually be interpreted as “shock” waves<sup>4</sup> when they are better understood. Though 8 times less sensitive than MGS, the Mars Climate Orbiter accelerometer may confirm such sudden changes.

### *Stationary Planetary Waves*

Figure 9 presents an example of stationary planetary waves. The plot shows density at the reference altitudes of 130 through 160 km versus longitude for the inbound leg of orbits 587 thru 626. The solid line through each set of data results from a wave five, least square fit to the data(+). The dashed lines are  $2\sigma$  error bars for model predictions. Results like these were used by the Accel Team during operations to make predictions for future orbits. Maximum density occurred near longitude  $100^\circ$  and local minima, about  $\frac{1}{2}$  of the maximum, occur about  $60^\circ$  on either side. Recall that the results at different altitudes do not include any overlap of the 40 second densities. The 40 second averaging does provide correlation between adjacent altitudes but not across two altitude changes. For these 40 orbits, the waves persist, in phase up to the highest altitudes. Similar results are seen on the outbound leg but the waves fade out at the highest two altitudes. At the lower altitudes, actual variations could be as large as a factor of three, and in the worst case scenario for operations, could occur on adjacent orbits. Clearly such large, persistent variations are of interest for the design of aerobraking spacecraft as well as for the operation of such missions. Similar wave structure existed in Phase 1<sup>5</sup> and throughout much of Phase 2. Such nearly stationary waves must be forced by surface topography but the correlation is not straight forward though there are persistent patterns.

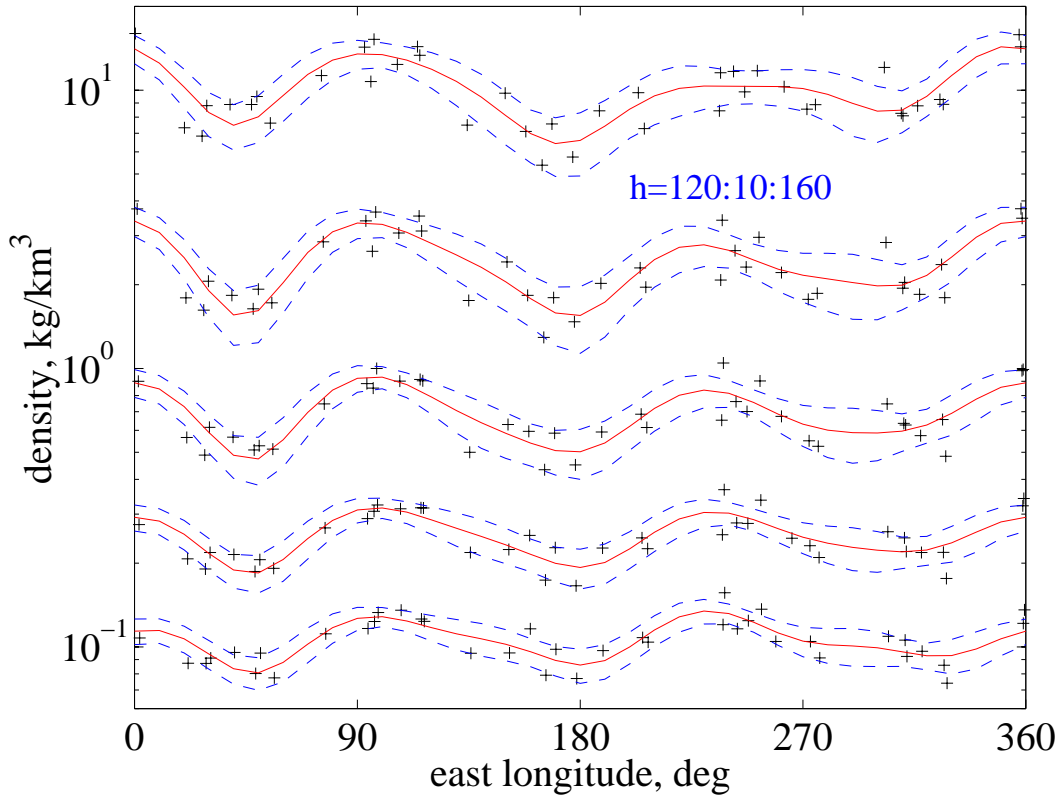


**Figure 9 Density variations at reference altitudes for orbits 587 through 626 and wave 4 models.**

### *Local Waves*

There were numerous orbits where accelerometer counts appeared to change nearly instantaneously.<sup>3</sup> Two examples are given in Figure 10 where  $\rho_7$  is shown for P41 and P114. Although earlier orbits, with the 1 sample every 8 seconds data rate, had shown large changes in density, P41 was the first orbit to show such a sudden change after the accelerometer data recovery rate was increased to 10 Nq. At about -90 seconds the density starts increasing at a higher rate than expected, decreases just before periapsis, and suddenly increases by 40% in a few seconds. On the other hand, P114 shows a sudden 60% decrease in acceleration just after periapsis. Because such phenomena were outside the range of atmospheric experiences, early attempt to explain these variations concentrated on s/c related phenomena. On board mass movement due to fuel sloshing and quasi-static SAM bending can be ruled out because such events will have time scales of a few seconds, and after the relative motion ends, the acceleration profile would return to only that due to drag. Accelerometer “sticking” is highly unlikely and would be expected to be repeated orbit to orbit. Further, sudden increases in

acceleration are almost always accompanied by excitation of the SAM as measured by the rate gyros, strongly suggesting a change in dynamics and not a sensor anomaly. Changes in gas-surface interaction were also considered. Momentum accommodation is assumed to be complete<sup>7</sup> on the entire s/c giving a drag coefficient near 2. If specular reflection is assumed, the drag coefficient would nearly double. Phenomena that could produce such dramatic changes might include condensation and evaporation of atmospheric gases on the s/c surface. Though considered unlikely, such possibilities have not been completely explored.

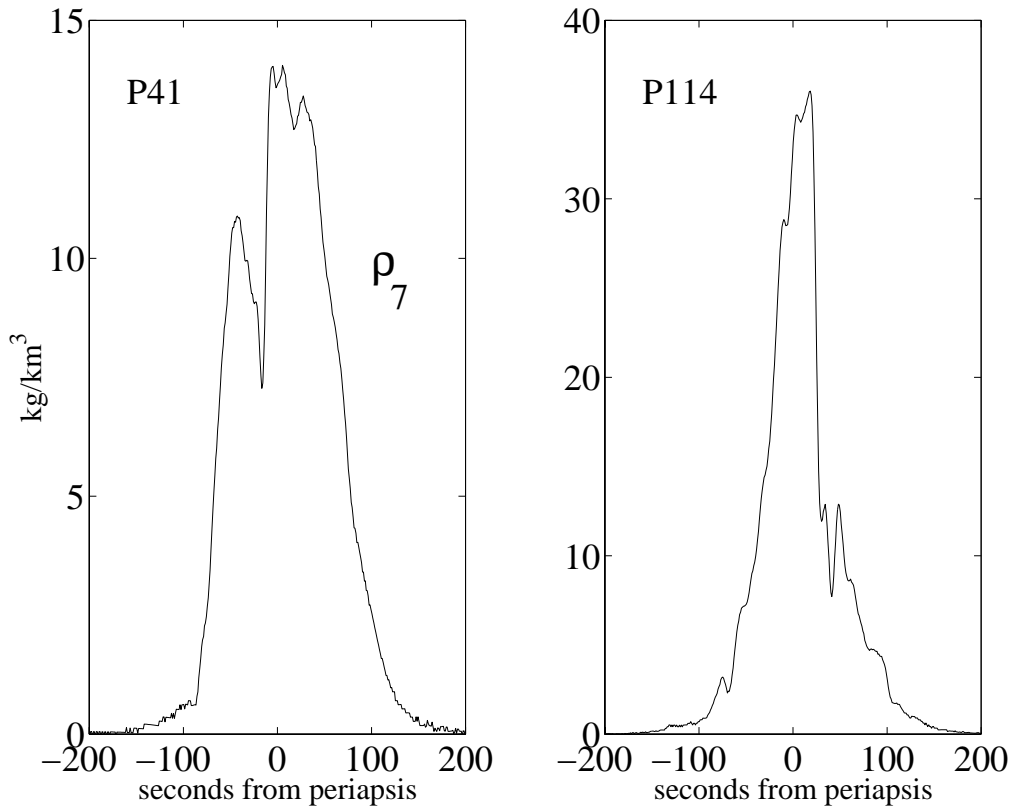


**Figure 10. Orbits 41 and 114 density,  $\rho_7$ .**

Orbit 58 is one orbit where the sudden jump in acceleration occurred at a low dynamic pressure. Note in Figure 3 that there is a clear change in  $\omega_x$  at the same time (near -90 seconds) that the counts increase. Figure 11 provides a view of the raw accelerometer data,  $\omega_x$  and  $\omega_y$  around -90 seconds. The bias has been removed from the raw data and it can be seen that the counts increase from 1.3 at -89 seconds to about 5 in less than 5 seconds. Polynomial fits (solid lines) to the rate data (dots) yield ratios of 5.4 and 4.6 for the angular acceleration on either side of  $t=-87$ . Data at the 4 times marked on the counts plot are not included in the polynomial fits. The vibration effects of the SAM after the change is evident in the upper 2 data sets. The straight forward conclusion from these results is that atmospheric density increased by about a factor of 4 to 5 on a very short spatial and temporal scale. At this time the altitude rate is -280 m/s and the down track velocity is 4.8 km/s.

More detailed analyses has been performed considering the effects of the quasi-static panel deflection of about  $1^\circ$  on all the aerodynamic coefficients, onboard angular momentum sources, and the possibility of zonal winds. The conclusion is unchanged.

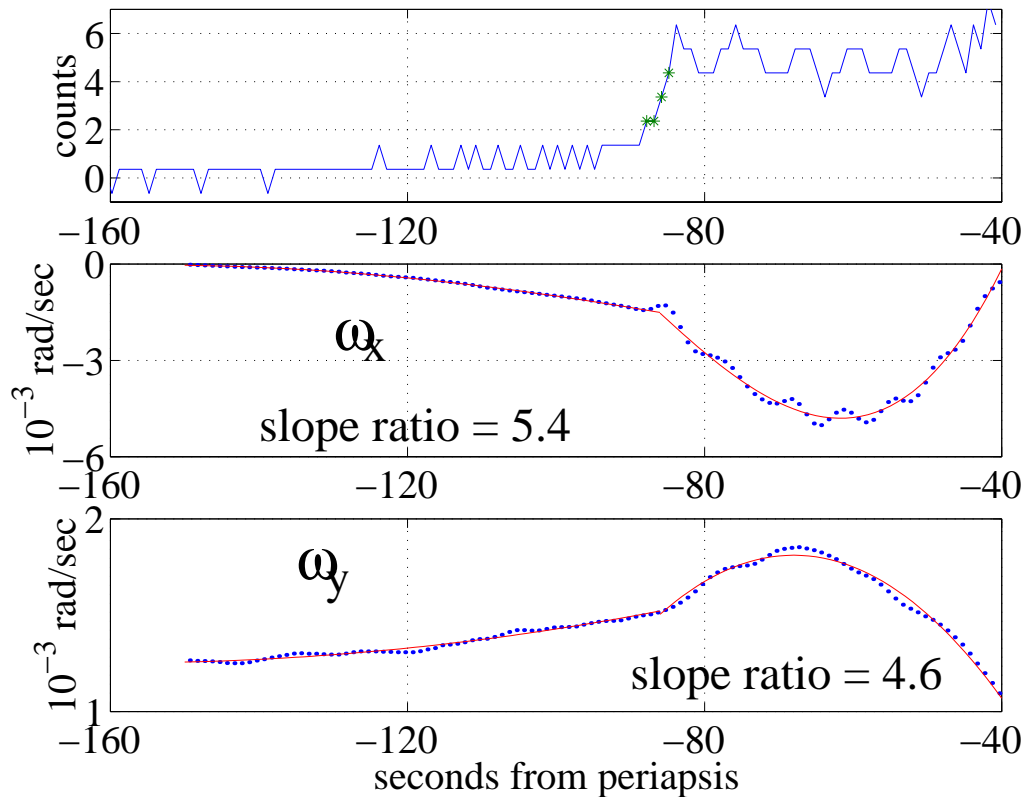


**Figure 11 Accelerometer counts,  $\omega_x$  and  $\omega_y$  for orbit 58.**

### Conclusions

Providing reliable archival data from the Mars Global Surveyor accelerometer has proven to be less than straight forward due primarily to the broken solar array. Methods have been developed that should minimize the impact on final data products. The resulting data provides a wealth of new information about the thermosphere of Mars. Persistent planetary scale longitudinal waves and large, short time and spatial scale transients are among the unexpected phenomena found during this mission. Such variations are yet to be explained by theoretical models, and lack of understanding of the fundamental physics will limit prediction capability for future missions. Nevertheless, the archived data from this mission will provide a basis for improving such models as well as improving empirical models.

Given the unexpected variations in the thermosphere, and our need to understand these variations for scientific, s/c design and operational reasons, it is recommended that future aerobraking missions routinely measure and archive quality accelerometer data to extend the data base to other seasons, latitudes, and solar cycle phases.

## Acknowledgments

This work was sponsored by the Mars Surveyor Operations Office, Jet Propulsion Laboratory (JPL), California Institute of Technology.

## References

- <sup>1</sup>Lyons, D.T., Beerer, J.G., Esposito, P., Johnston, M.D., “Mars Global Surveyor: Aerobraking Mission Overview,” *Journal of Spacecraft and Rockets*, Vol. 36, No. 3, May-June, 1999, pp 307-313.
- <sup>2</sup>Culp, R.D. and Stewart, I, “Time-Dependent Model of the Martian Atmosphere for use in Orbit Lifetime and Sustenance Studies,” *Journal of the Astronautical Sciences*, Vol. 32, No. 3, July-September, 1984, pp329-341.
- <sup>3</sup>Tolson, R.H., Keating, G.M., Cancro, G.J., Parker, J.S., Noll, S.N., and Wilkerson, B.L., “Application of Accelerometer Data to Mars Global Surveyor Aerobraking Operations,” *Journal of Spacecraft and Rockets*, Vol. 36, No. 3, May-June, 1999, pp. 323-329.
- <sup>4</sup>Justus, C.G., James, B.F., and Johnson, D.L., “Mars Global Reference Atmospheric Model (Mars-GRAM 3.34): Programmer’s Guide,” NASA TM 108509, May 1996.
- <sup>5</sup>Keating, G.M., et al., “The Structure of the Upper Atmosphere of Mars: In Situ Accelerometer Measurements from Mars Global Surveyor,” *Science*, Vol. 279, March 13, 1998, pp. 1672-1675.
- <sup>6</sup>Cancro, G.J., Tolson, R.H., & Keating, G.M., “Operational Data Reduction Procedure for Determining Density and Vertical Structure of the Martian Upper Atmosphere from Mars Global Surveyor Accelerometer Measurements,” NASA/CR-1998-208721, October 1998.
- <sup>7</sup>Wilmoth, R.G., Rault, D.F., Cheatwood, F.M., Engelund, W.C., and Shane, R.W., “Rarefied Aerothermodynamic Predictions for Mars Global Surveyor,” *Journal of Spacecraft and Rockets*, Vol. 36, No. 3, May-June, 1999, pp. 314-322.

## Appendix

The broken SAM demanded the attention of mission operations from orbit 15 until the end of aerobraking. It continues to play a role in the interpretation of accelerometer data to improve thermospheric models. It is therefore essential to understand and quantify the dynamics of the SAM. SAM deflection measurements and s/c angular body rate measurements provided the best information on SAM dynamics.

To determine density, the deflection of the SAM was modeled as a non-linear spring.<sup>6</sup> A solar sensor on the panel provided measurements of panel deflection ( $\pm 0.5^\circ$ ) on numerous but not all orbits. The calculated and observed deflection compared within

1.5° throughout the mission. Since 1° change in panel position produces less than 2% change in  $C_z$ , these results suggest that any change in spring constant would not produce a significant error in recovered density.

The operations team performed an orbit by orbit FFT of  $\omega_x$  to determine if the high frequency component near 0.16 Hz had changed frequency significantly. Such a change would have indicated a variation in panel stiffness and may have been cause for changing aerobraking strategy. Additional periodic test was done by the GWU Accel Team to verify that the dynamical properties had not changed in more subtle ways that might influence density recovery. These test involved studies of the frequency of vibration as a function of the quasi-static panel position and the determination of vibration frequency and damping with small aerodynamic loading.

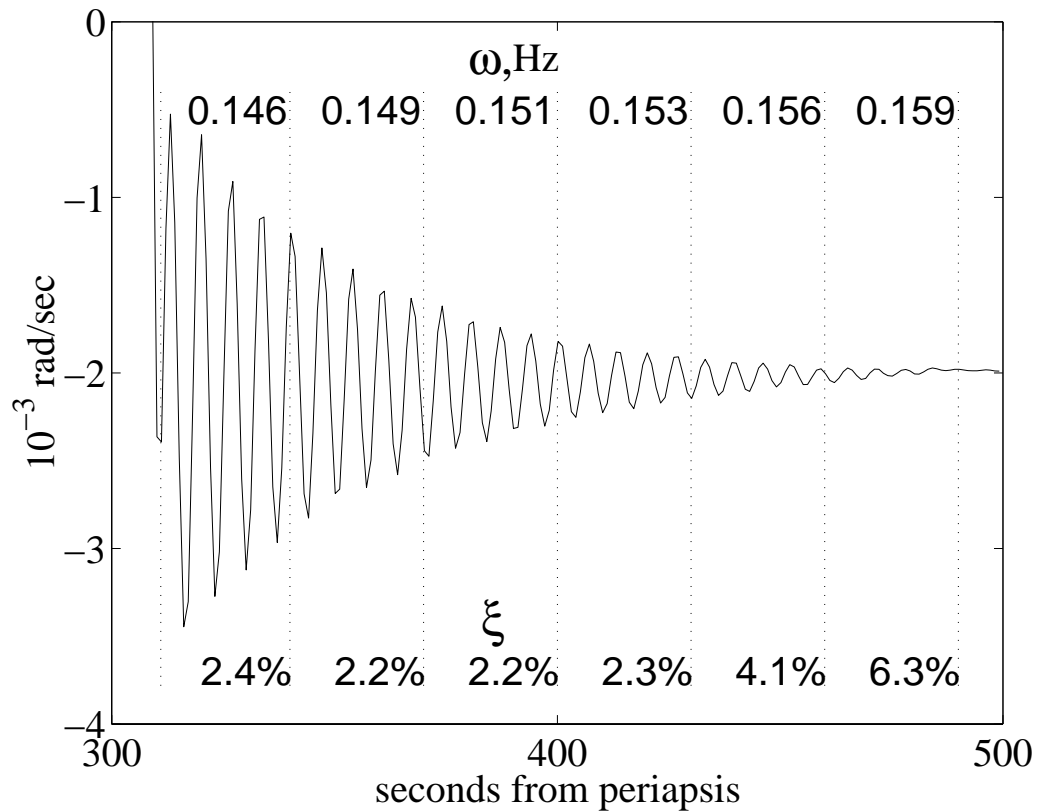


**Figure A Frequency and damping for SAM vibration on orbit 670.**

Figure A shows an example of the latter type study for orbit 670. During this orbit a thruster firing at 308 sec. excited the SAM into vibration. The vibration is seen to nearly damp out by the time of the next firing at about 510 sec. A modal identification analysis was performed on these data in 30 second blocks starting at 310 and ending at 460 seconds as indicated by the dotted vertical lines. The resulting natural frequency of vibration is shown at the top of the figure and the damping coefficient as a percent of critical is shown at the bottom. The non-linearity in the cracked SAM is clearly evident

by the monotone decrease in frequency with amplitude. In other words the stiffness of the crack decrease with amplitude. Damping is light and appears to be essentially constant until the amplitude decreases to about  $10^{-4}$ , and then damping increases rapidly.

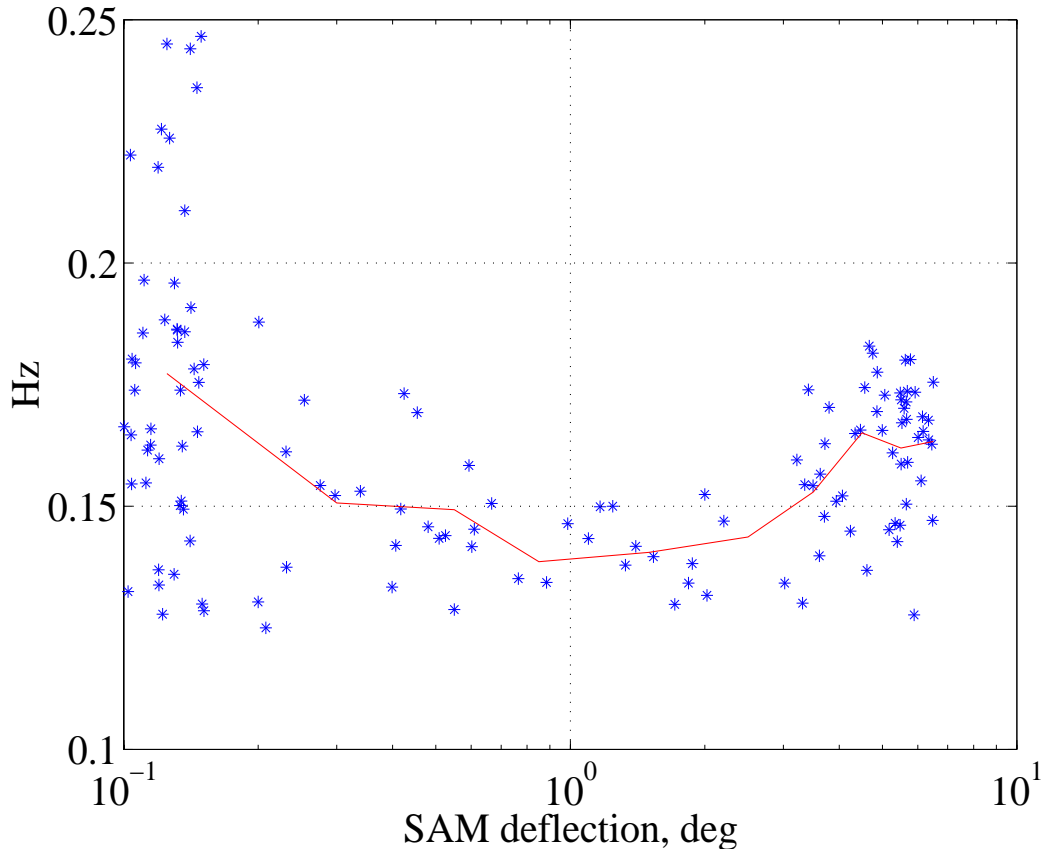


**Figure B Variation of SAM vibration frequency with quasi-static panel deflection for orbit 746.**

Another type of analysis determined SAM vibration frequency on a shorter time scale and while the s/c was under significant dynamic pressure. This is a difficult analysis because the phase of the vibration would often change dramatically in a short time span, due perhaps to local atmospheric density variation or panel self-interference. The simple approach of measuring the times between same direction, adjacent zero crossings of high pass filtered  $\omega_x$  data provided a crude measure of frequency. Figure B shows the results for orbit 746 as the individual points. All data for panel deflections less than  $0.1^\circ$  are scaled to plot between  $0.1^\circ$  and  $0.15^\circ$ . The solid line connects the means in 10 bins spread from  $0.1^\circ$  to  $7^\circ$ . This orbit was selected because it provides a large SAM deflection and minimal SAM vibration phase changes during the orbit. At low panel deflection (i.e. dynamic pressure) the frequency is 0.175 Hz, about 10% above the maximum frequency in Figure A. As panel deflection increases, the frequency decreases

indicating a softening spring perhaps due to slippage of the broken composite sheet along the crack. The lowest frequency here is very close to the lowest in Figure A. Above a  $3^\circ$  deflection the spring begins to stiffen. On some orbits, vibration frequency about quasi-static displacements greater than  $7^\circ$  reaches as high as 0.2 Hz, indicating a substantial hardening perhaps due to SAM crack closure and additional structure coming into play.

These tests were performed periodically throughout aerobraking and gave sufficiently similar results that it was concluded that SAM dynamical properties did not change significantly.